Light-scattering study of a supercooled epoxy resin

L. Comez, D. Fioretto, L. Palmieri, and L. Verdini
INFM and Department of Physics, University of Perugia, via Pascoli, 06123 Perugia, Italy

P. A. Rolla
INFM and Department of Physics, University of Pisa, Piazza Torricelli 2, 56126 Pisa, Italy

J. Gapinski,* T. Pakula, A. Patkowski,* W. Steffen, and E. W. Fischer
Max-Planck-Institut für Polymerforschung, Ackermannweg 10, 55128 Mainz, Germany
(Received 7 August 1998; revised manuscript received 8 April 1999)

The dynamics of the fragile glass-forming liquid diglycidyl ether of bisphenol-A was studied by depolarized Rayleigh-Brillouin light-scattering and photon correlation spectroscopy above the glass transition, in the temperature range from 261 to 473 K and in the frequency range from 1 Hz to 300 GHz. The structural ($\alpha-$) relaxation process was revealed and no signature of the secondary relaxation previously evidenced by dielectric spectroscopy at about 0.1 GHz was observed. The characteristic time of the α process differs from that determined by dielectric spectroscopy of an amount, which increases with increasing temperature. The relaxation times were compared with viscosity data to test the predictions of the classic Stokes-Einstein-Debye model. The $\tau \propto \eta$ behavior was verified for dielectric data, while a fractional power law of viscosity $\tau \propto \eta^{0.89}$ was obtained for light-scattering relaxation times, extending over more than seven decades in viscosity and time. This deviation of light scattering from viscosity data could be interpreted in terms of cooperative motion in the supercooled liquid with a characteristic length $\xi_a \propto (T-T_0)^{-\nu}$ where $T_0 = 229$ K is the Vogel temperature and ν is close to $\frac{2}{3}$ which is consistent with the prediction of the fluctuation theory of glass transition. [S1063-651X(99)04009-X]

PACS number(s): 64.70.Pf, 78.35.+c, 61.20.Lc, 83.50.Fc

I. INTRODUCTION

The supercooled state of matter has been the subject of an extensive experimental and theoretical work aimed at the understanding of the microscopic origin of the glass transition. One of the primary features of the supercooled state is the marked increase of the shear viscosity η with decreasing temperature in a narrow temperature range [1]. The gradual cessation of the viscous flow of a liquid is associated with the development of shear elasticity. In this regime, the Maxwell model of viscoelasticity provides the relationship $\tau_s = \eta / G_\infty$ between the relaxation time τ_s of shear stress and shear viscosity η, where G_∞ is the unrelaxed shear modulus. This relaxation of stress in the liquid corresponds to the rearrangement of molecules and is usually referred to as structural (or α) relaxation. By cooling the liquid, when the structural relaxation time becomes longer than the time of the experiment, the molecules cannot rearrange completely during the experiment and the system appears to be frozen in a disordered state, becoming a glass. The glass transition temperature T_g is conventionally identified by $\tau_s = 100$ s or by a viscosity attaining 10^{13} P. In the transition from the liquid to the glassy phase, the dynamics of the structural relaxation covers an exceptionally large time window ranging from about 10^{-12} s in the liquid phase up to 100 s at the glass transition.

For a long time the study of the glass transition has been focused on a narrow temperature range close to T_g, looking for some singularity typical of a phase transition. On approaching the glass transition, the increase of the structural relaxation time with decreasing temperature is well represented by the phenomenological Vogel-Fulcher-Tammann (VFT) law [2],

$$\tau(T) = \tau_0 e^{B/(T-T_0)}, \tag{1}$$

which was interpreted in terms of the reduction of free volume for the diffusion [3] and, more recently, of enhancement of cooperative motions [4,5], or of a percolation phase transition between liquid and solidlike clusters [6].

The experimental verification of Eq. (1) and the predictions of the theories become more and more difficult for temperatures lower than T_g. In fact, after a small change of temperature, the sample must be equilibrated, without crystallization, for a time longer than τ_s. In a very careful dielectric measurement performed recently on a polymeric glass former [7], the structural relaxation up to 10^7 s was measured and a smooth $\tau(T)$ behavior well described by a single VFT law was reported. The absence of any singularity seems to exclude the presence of a phase transition at T_g.

In recent years, the development of the mode-coupling theory (MCT) (for a review, see Ref. [8]) caused a renewed interest in the theoretical and experimental study of glass-forming liquids. The crucial point of the theory is the existence of a dynamical phase transition located at a critical temperature T_c between the melting and the glass-transition temperature. Close to this temperature, nonlinearities in the dynamics of the system are responsible for the structural ar-

*Also at Institute of Physics, A. Mickiewicz University, Poznan, Poland.

rest, i.e., for a power-law divergence of the viscosity, a square root singularity of the Debye-Waller factor, and many other features that have been extensively tested on simple glass-forming systems [8–10]. One of the major merits of the MCT in the study of supercooled systems has been to move the attention from T_g to 50–100 K above T_g, looking for the dynamical onset of the glass transition.

At temperatures higher than T_g the rotational diffusion correlation time τ can be related to the macroscopic viscosity η and temperature by the Stokes-Einstein-Debye (SED) equation [11]

$$\tau = \frac{V_h \eta}{kT}. \tag{2}$$

This equation was written for the diffusion of a single macroscopic particle in a viscous liquid but it was found to hold also for the diffusion at the molecular level in ordinary liquids at high temperature, with the eventual addition of a small constant value τ_0, which accounts for the nonzero correlation time when η goes to zero, and by considering the volume V_h as an effective volume, which accounts for interaction effects. A marked change of both rotational and translational diffusion mechanisms was observed in organic liquids, corresponding to a breakdown of the SED diffusion law (see, for instance, Refs. [12–20], and references therein). This phenomenon was localized in a relatively narrow temperature range corresponding to $T/T_g = 1.20-1.28$, where also the critical temperature T_c was located. Moreover, for those systems having also a secondary relaxation, the splitting of the primary ($\alpha-$) and secondary ($\beta-$) relaxation occurs in the same temperature range [12]. It can be thought that this dynamic transition is the physically significant feature of the supercooled liquid, while the glass transition is mainly related to the way the state is prepared (cooling rate) rather than to a fundamental change in the state of matter.

Convincing experimental evidence of the existence of dynamic transition in supercooled liquids has also been obtained by a careful investigation of the dielectric response of glass-forming liquids [21–24]. Also in this case the change in the temperature behavior of the α-relaxation time was observed to coincide with the bifurcation of α and β relaxations [23,24].

The analysis of this complex scenario characterizing the dynamics of a supercooled system requires the use of spectroscopic techniques covering wide frequency and temperature ranges. Moreover, there is a great interest in comparing the results obtained by different spectroscopic techniques to establish the extent to which the same relaxation process is probed by different observables, i.e., to check the possible existence of some ''universal'' behavior in the dynamics of supercooled systems. Light-scattering and dielectric techniques are particularly suitable for this purpose since they can cover the whole dynamics of the structural relaxation from the liquid phase down to the glass transition, being also sensitive to subglass relaxation processes. In recent years, depolarized light scattering has been extensively used to test the predictions of the mode-coupling theory [9,10,25], mainly in the high-temperature ($T > T_c$), high-frequency ($f > 10^8$ Hz) regime. For temperatures approaching T_g this technique was also employed to test the predictions of the fluctuation theory of glass transition [5,26] giving evidence of a correlation length whose value diverges when approaching the Vogel temperature T_0 of the system.

The aim of the present paper is to investigate the temperature behavior of the structural relaxation of a glass-forming system revealed by depolarized light scattering DLS in comparison with the results of viscosity and dielectric spectroscopy (DS) measurements performed on the same system. The epoxy resin diglycidyl ether of bisphenol-*A* (DGEBA) here employed is particularly appropriate for such investigation since it is a fragile [27] glass former, which does not exhibit any appreciable crystallization; also, at the slowest cooling rates, it gives a strong depolarized light signal appropriate for depolarized light-scattering studies and it has a sufficiently large dipole moment associated with each of the two epoxy rings of each molecule, which allowed a detailed dielectric investigation in a wide frequency and temperature range [28,29]. Dielectric investigation revealed a secondary relaxation whose temperature behavior is strongly affected by the glass transition. Moreover, dielectric spectra showed a well defined onset of the α relaxation at a temperature 93 K higher than T_g, a signature of some dynamic transition [30,5] occurring in the system. In the present paper we report the results of depolarized light-scattering and viscosity experiments performed on DGEBA in the frequency range of 1 Hz–300 GHz and for temperatures between 261 and 473 K. To access this wide frequency range we combined the spectra obtained from a tandem Fabry-Perot interferometer (T-FPI) of different free spectral ranges, a confocal Fabry-Perot interferometer (C-FPI), and results from a photon correlation spectroscopy (PCS) experiment. The temperature evolution of the structural relaxation time obtained by these techniques is compared with the viscosity to test the validity of the SED law, and both the relaxation time and the shape parameters of the spectra are compared with the dielectric ones, in order to test how these two different techniques account for the same structural relaxation.

II. EXPERIMENT

The epoxy resin was a commercial sample (EPON828 by Shell Co.) of liquid DGEBA with an epoxy equivalent weight of about 190, corresponding to $n = 0.1$ in the chemical formula reported in Fig. 1(a). The calorimetrically determined glass-transition temperature of the system is $T_g = 257$ K, also confirmed by dielectric measurements [28]. The sample was filtered through a 0.22-μm Millipore filter at a temperature of 70 °C and distilled into dust-free light-scattering round cells, 10-mm inner diameter, which were flame-sealed afterwards. These samples kept at room temperature for several months showed no trace of crystallization.

To obtain wide frequency range spectra, the horizontally polarized (VH configuration) light was analyzed by means of three different spectrometers. A Sandercock-type $(3+3)$-pass tandem Fabry-Perot interferometer [31], characterized by a finesse of about 100 and a contrast ratio greater than 5×10^{10} was used to collect I_{VH} spectra in the 0.3–300-GHz region. The light sources were an Ar^+ laser operating in a single mode of the 514.5-nm line and a 532-nm Nd:YAG laser (coherent). The back-scattering geometry was em-

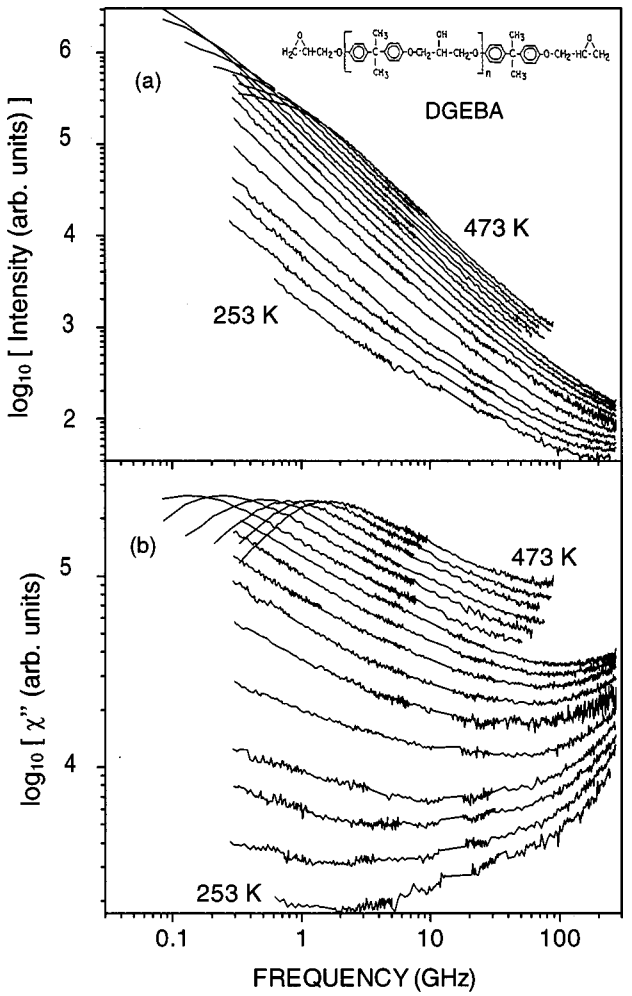

FIG. 1. (a) Depolarized Rayleigh-Brillouin spectra measured by means of the tandem Fabry-Perot interferometer. Temperatures from top to bottom are 473, 453, 433, 413, 393, 373, 353, 343, 333, 323, 313, 298, 283, 273, 263, and 253 K. (b) Susceptibility spectra corresponding to the data of Fig. 1(a), calculated by Eq. (3).

ployed to avoid intense contributions to the spectra coming from transverse acoustic modes. The occurrence and the temperature evolution of these modes for temperatures lower than 313 K was revealed for a different scattering geometry and reported in a previous paper [32]. Four different mirror separations corresponding to different free spectral ranges (FSR) of 7.5, 10, 37.5, and 300 GHz were used to obtain spectra in the whole frequency range. In the case of FSR $=7.5$ and 10, in order to avoid distortions of the spectra, narrow interference filters can be used that suppress the light coming from the higher orders of the response function of the tandem interferometer. The use of these filters has been demonstrated to be crucial in glass-forming systems at low temperature, i.e., between $1.2T_g$ and T_g [33]. In the present experiment the filter was not necessary since the investigated temperatures are higher than $1.2T_g$. At these temperatures, a great part of the α relaxation is within the frequency window of the experiment and the spectrum fastly decreases with frequency, thus substantially reducing the overlap effects. The sample was cooled by nitrogen vapor evaporated from liquid nitrogen and heated by a heater controlled by a Thor Cryogenics 3010 II temperature controller. The temperature was measured by a copper-constantane thermocouple placed close to the sample and the temperature fluctuations were kept within ± 0.1 °C.

A Burleigh confocal interferometer, FSR 750 MHz, was used to obtain depolarized spectra at a scattering angle of 90°, in the frequency range between 10 and 350 MHz. The incident light (single mode, $\lambda = 532$ nm) was supplied by a Nd:YAG laser (ADLAS).

A Brookhaven BI-9000AT correlator was used for PCS measurements to study the low-frequency (long-time) dynamics of the system. PCS measurements were carried out in the range $10^{-6}-1$ s and for temperatures from 261 to 281 K. The backscattering configuration was exploited, using the same geometry and the same experimental setup adopted for the tandem Fabry-Perot experiments. In this case, the light scattered from the sample was directly sent to the photomultiplier, without passing through the Fabry-Perot interferometer.

Dynamic mechanical measurements were performed by means of the Rheometrics RMS 800 mechanical spectrometer. Shear deformation was applied under condition of a controlled deformation amplitude, always remaining in the range of the linear viscoelastic response of studied samples. Frequency dependencies of the storage (G') and loss (G'') shear modulus were measured at various temperatures. A geometry of parallel plates was used below 25 °C, with plate diameters of 6 nm, whereas at higher temperatures the measurements were performed with the cone-plate geometry of a 50-mm diameter. In the case of the plate-plate geometry the gap between plates (sample thickness) was about 1 mm. Experiments have been performed under dry nitrogen atmosphere.

III. RESULTS

A. Tandem-FPI measurements

In the case of tandem measurements, spectra of different frequency ranges at the same temperature were joined by multiplying their intensities by an appropriate constant factor and matching the overlap ranges [34]. The composite T-FPI spectra $I_{\mathrm{VH}}(\omega)$ are reported in Fig. 1 where it is possible to see that the high-temperature spectra exhibit a broad central peak, which extends up to the highest measured frequencies. With decreasing temperature the spectra become narrower and the characteristic frequency of the structural relaxation moves out of the frequency window. At lower temperatures it will be measured by the confocal and photon correlation spectroscopies.

In the same figure the susceptibility spectra $\chi''(\omega)$ are also shown, obtained from the spectra through the relationship

$$\chi''(\omega) = \frac{I_{\mathrm{VH}}(\omega)}{[n(\omega)+1]}, \tag{3}$$

where the Bose factor can be approximated by $[n(\omega)+1] = k_B T/\hbar\omega$ in the frequency and temperature ranges of interest. The relaxation behavior of the system is clearer shown by the susceptibility spectra rather than by the intensity spectra.

TABLE I. Parameters obtained by fitting Eq. (4) to spectra of Fig. 2.

T (K)	a	b	$\chi_{min}/1000$	f_{min} (GHz)
298	0.79	0.23	11.3	33.3
313	0.40	0.39	17.1	36.5
323	0.40	0.42	22.1	46.5
333	0.48	0.39	27.0	64.3
343	0.40	0.43	31.5	83.4
353	0.43	0.40	36.5	110

For temperatures higher than 373 K, the maximum of the peak related to the structural relaxation is visible in the tandem susceptibility spectra and the characteristic time and the shape parameters of the relaxation can be directly calculated from these spectra, as described below. For lower temperatures, the maximum is located at lower frequencies and confocal spectra were required to enlarge the frequency resolution. In the tandem spectra, two distinct regions can be recognized. The region where susceptibility decreases with increasing frequency is dominated by the high-frequency part of the structural relaxation. The almost linear behavior in the log-log plot suggests a power-law behavior of $\chi''(\omega)$ of the type $\chi''(\omega) \propto \omega^{-b}$ to hold in this region. The high-frequency region, where susceptibility increases with frequency, is located at frequencies lower than that of the boson peak of disordered systems, and can also be described by a power law, i.e., a $\chi''(\omega) = A\omega^{a}$. According to the mode-coupling theory [8], the region of the minimum of susceptibility can be interpolated by the equation

$$\chi''(\omega) = \frac{\chi''_{min}}{a+b}\left[b\left(\frac{\omega}{\omega_{min}}\right)^{a} + a\left(\frac{\omega}{\omega_{min}}\right)^{-b}\right]. \qquad (4)$$

MCT makes nontrivial predictions for the values of the minimum of susceptibility χ''_{min}, of the frequency of the minimum ω_{min}, and of the shape parameters a and b. In particular, the values of the parameters a and b must be temperature independent for $T > T_c$ and fulfill the relationship $\lambda = \Gamma^2(1-a)/\Gamma(1-2a) = \Gamma^2(1+b)/\Gamma(1+2b)$, where $0 < a < 0.395$, $0 < b < 1$, Γ is the gamma function, and λ is the ''exponent parameter'' that fixes the values of all exponents of the theory. The values of the parameters obtained by fitting Eq. (4) to the spectra are reported in Table I. It can be noticed that for $T > 300$ K the shape parameters are almost temperature independent, as predicted by the MCT. On the other hand, the pair of values of a and b does not satisfy the above relationship. Similar deviations from the predictions of the idealized version of MCT were previously revealed by light-scattering measurements of both fragile and nonfragile systems and attributed to the influence of low-frequency vibrations (boson peak) on the MCT β-relaxation region [25]. Moreover in the dynamics of DGEBA some internal degrees of freedom play a non-negligible role [28], so that this system is not the best candidate for a quantitative test of MCT predictions. In addition, the spectra of Fig. 2 are not extended enough in the high-frequency region to cover both the MCT β region and the boson peak. On the other hand, the low-frequency part of the spectra is sufficiently well defined

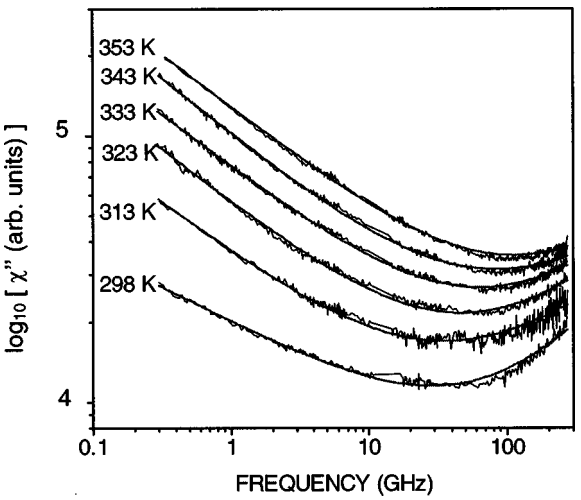

FIG. 2. Susceptibility spectra (thin line) fitted by Eq. (4) (thick solid line).

to give confidence to the values of the shape parameter b. This value is needed both for a comparison with dielectric data and to guide the analysis of light-scattering spectra at lower frequencies. In fact, the coincidence of the shape of the C-FPI and T-FPI spectra in the overlapping region gives an important constraint in fitting the confocal spectra.

B. Confocal-FPI measurements

The confocal interferometer is not in a tandem configuration so that overlap effects must be taken into account. In the case of scattering from dilute solutions, the experimental spectra can be fitted by a single Lorentzian convoluted with the periodic instrumental function. In the case of DGEBA, a single Lorentzian fit gives considerable deviations from measured data, indicating that the single relaxation time approximation is not suitable to describe the dynamics of the epoxy system. A sum of Lorentzians with different relaxation times [10] has been demonstrated to be more appropriate to take into account the stretching of the structural relaxation. In the present case, in order to be consistent with the elaboration procedure of dielectric and photon correlation data, we preferred a single-stretched Lorentzian to describe both the confocal and the tandem FPI data. The stretched Lorentzian $I_{VH}(\omega)$ was obtained by the Havriliak-Negami (HN) [35] relaxation function,

$$I_{VH}(\omega) = \frac{I_0}{\omega}\,\mathrm{Im}\{[1 + (i\omega\tau_{HN})^{\alpha}]^{-\gamma}\}, \qquad (5)$$

where τ_{HN} is the relaxation time, and α and γ are shape parameters. In the low- and high-frequency limits the HN function leads to two power laws characterized by the exponents $m = \alpha$ and $-n = -\alpha \cdot \gamma$, respectively. The coincidence of the shape of confocal and tandem spectra was obtained by fixing the values of n to those determined by fitting Eq. 4 to the tandem spectra.

A baseline I_B was added to Eq. (5) to account for high-frequency contributions to the spectra and the obtained expression, convoluted with the instrumental function, was fitted to the confocal spectra by means of the Levenberg-Marquardt algorithm.

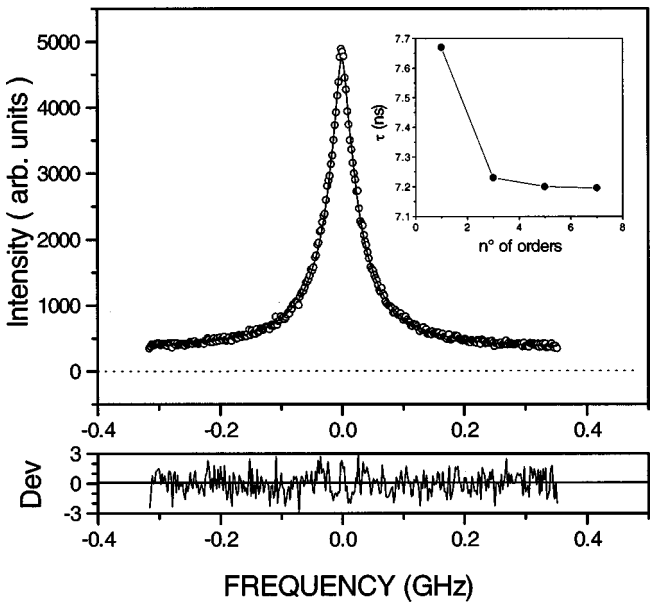

FIG. 3. Depolarized Rayleigh-Brillouin spectrum measured at 343 K by means of the confocal Fabry-Perot interferometer, fitted by Eq. (5) (solid line) and corresponding deviation plot dev$=(I_{\mathrm{exp}}-I_{\mathrm{fit}})I_{\mathrm{exp}}^{-1/2}$. In the inset, the value of the relaxation time τ obtained by the fit as a function of the total number of orders used in the convolution procedure with the instrumental function.

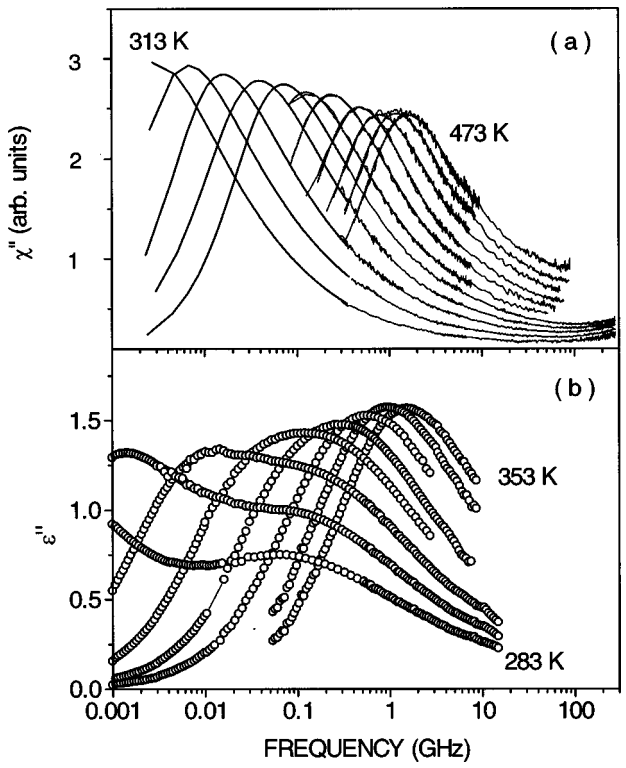

FIG. 4. (a) Composed confocal and tandem Fabry-Perot susceptibilities. Temperatures are 313, 323, 333, 343, 353, 373, 393, 413, 433, 453, and 473 K. (b) Dielectric spectra from Ref. [28], taken at 283, 293, 303, 313, 323, 333, 343, and 353 K.

Figure 3 shows the result of fitting Eq. (5) to a spectrum taken at 343 K where, in the convolution procedure, two neighboring orders were taken into account on each side of the spectrum to remove the overlap effect. The goodness of the fit is also confirmed by the residuals, which show no appreciable systematic deviations. A further test of the quality of the fit was obtained by repeating the procedure after having increased the number of neighboring orders in the convolution. The behavior of one parameter, i.e., of the relaxation time τ, is shown in the inset of Fig. 3 as a function of the number of orders. It can be seen that for a number higher than five (two orders for each side of the central peak) the value of the parameters of Eq. (5) does not change appreciably. Fitting with more than five orders changes only the value of the baseline I_B. The value of I_B goes to zero (becomes lower than the data error) using more than 24 neighboring orders in the convolution, which corresponds to taking into account the contribution of light scattered up to 18 GHz apart from the central line. The presence of a considerable amount of light scattered at this frequency is confirmed by the T-FPI spectra of Fig. 1.

In Fig. 4(a) the confocal spectra obtained by this fitting procedure are reported together with the T-FPI ones. For sake of comparison, some of the dielectric spectra previously obtained [28] are reported in Fig. 4(b). The maximum of the susceptibility in light-scattering spectra is now apparent also for temperatures lower than 370 K, and its evolution with temperature gives the behavior of the structural relaxation time. The relaxation parameters obtained by fitting the spectra with Eq. (5) are reported in Table II and the corresponding spectra are shown as thicker lines in the figure. It can be seen that the low frequency of the confocal spectrum measured at $T=313$ K is missing due to experimental limitations. Therefore, in the fitting procedure we fixed the value to 0.92 obtained by the interpolation of the data at higher and lower temperatures. Similarly, for the two spectra at 373 and 393 K, where the low frequency part of the susceptibility peak is out of the experimental window, the value of the parameter α of Eq. (5) was kept constant, equal to its limiting value $\alpha=1$, corresponding to a Cole-Davidson relaxation function. In fact, $\alpha=1$ is the high temperature-limiting value obtained by fitting the confocal spectra up to 353 K. Moreover, this same value was obtained by the HN fit of the four high-temperature spectra in the range 413–473 K, within a standard deviation of about 3%. On this basis, in order to get more reliable values of the other fitting parameters, the value of α was kept equal to 1 also in this high-temperature region.

C. PCS measurements

It is not possible to extend the dynamical window of the light-scattering studies using interferometric techniques to lower frequencies, because of the finite linewidth of the laser line and the limited resolution of the FPI. For frequencies lower than a few MHz a time-domain technique, i.e., the photon correlation spectroscopy, has to be used.

In the photon correlation spectroscopy, when the homodyne technique is used, the time correlation function of the scattered intensity $G^{(2)}(t)=\langle I(t)I(0)\rangle$ is measured. In the present experiment we used the back-scattering VH geometry, which is the same as the one adopted in the T-FPI experiment. In this configuration a considerable amount of stray light comes from imperfections of the lenses and of the cell, which is partially stopped by the crossed polarizer in the scattered beam. The question could arise if the heterodyne

TABLE II. Parameters of the α relaxation obtained from the analysis depolarized light spectra.

T (K)	τ_{HN} (s)	m	n	τ_{KWW} (s)	β
261	$(2.35\pm0.2)\times10^{-1}$	0.82 ± 0.04	0.41 ± 0.02	$(9.15\pm0.16)\times10^{-2}$	0.51 ± 0.01
263	$(5.1\pm0.5)\times10^{-2}$	0.85 ± 0.04	0.45 ± 0.02	$(2.15\pm0.02)\times10^{-2}$	0.55 ± 0.01
265	$(1.65\pm0.2)\times10^{-2}$	0.83 ± 0.03	0.47 ± 0.02	$(7.17\pm0.05)\times10^{-3}$	0.57 ± 0.01
267	$(7.3\pm0.7)\times10^{-3}$	0.84 ± 0.03	0.43 ± 0.02	$(2.64\pm0.03)\times10^{-3}$	0.55 ± 0.01
269	$(2.8\pm0.2)\times10^{-3}$	0.83 ± 0.02	0.41 ± 0.02	$(9.63\pm0.1)\times10^{-4}$	0.57 ± 0.01
271	$(9.1\pm0.8)\times10^{-4}$	0.83 ± 0.02	0.43 ± 0.02	$(3.50\pm0.03)\times10^{-4}$	0.54 ± 0.01
273	$(3.2\pm0.3)\times10^{-4}$	0.86 ± 0.02	0.42 ± 0.03	$(1.20\pm0.08)\times10^{-4}$	0.54 ± 0.02
275	$(1.39\pm0.15)\times10^{-4}$	0.86 ± 0.02	0.42 ± 0.03	$(5.2\pm0.1)\times10^{-5}$	0.55 ± 0.01
277	$(6.1\pm0.6)\times10^{-5}$	0.86 ± 0.03	0.47 ± 0.03	$(2.7\pm0.4)\times10^{-5}$	0.58 ± 0.05
279	$(4.0\pm0.4)\times10^{-5}$	0.88 ± 0.03	0.43 ± 0.04	$(1.5\pm0.2)\times10^{-5}$	0.57 ± 0.06
281	$(2.1\pm0.2)\times10^{-5}$	0.83 ± 0.04	0.42 ± 0.04	$(7.3\pm1.1)\times10^{-6}$	0.52 ± 0.06
313	$(1.0\pm0.1)\times10^{-7}$	0.92	0.39 ± 0.01	$(3.3\pm0.4)\times10^{-8}$	0.51 ± 0.01
323	$(4.5\pm0.4)\times10^{-8}$	0.98 ± 0.06	0.42 ± 0.01	$(1.4\pm0.2)\times10^{-8}$	0.53 ± 0.02
333	$(1.8\pm0.1)\times10^{-8}$	0.96 ± 0.04	0.39 ± 0.02	$(5.5\pm0.6)\times10^{-9}$	0.53 ± 0.01
343	$(7.8\pm0.5)\times10^{-9}$	0.93 ± 0.03	0.43 ± 0.01	$(2.6\pm0.3)\times10^{-9}$	0.53 ± 0.01
353	$(4.2\pm0.4)\times10^{-9}$	0.98 ± 0.01	0.40 ± 0.02	$(1.3\pm0.3)\times10^{-9}$	0.53 ± 0.01
373	$(2.0\pm0.3)\times10^{-9}$	1	0.43 ± 0.02	$(6.1\pm0.8)\times10^{-10}$	0.54 ± 0.02
393	$(1.0\pm0.1)\times10^{-9}$	1	0.43 ± 0.02	$(3.6\pm0.5)\times10^{-10}$	0.54 ± 0.02
413	$(5.7\pm0.5)\times10^{-10}$	1	0.47 ± 0.01	$(2.3\pm0.3)\times10^{-10}$	0.59 ± 0.02
433	$(3.5\pm0.4)\times10^{-10}$	1	0.48 ± 0.01	$(1.4\pm0.2)\times10^{-10}$	0.60 ± 0.02
453	$(2.3\pm0.2)\times10^{-10}$	1	0.50 ± 0.01	$(9.9\pm1.5)\times10^{-11}$	0.62 ± 0.02
473	$(1.7\pm0.2)\times10^{-10}$	1	0.50 ± 0.01	$(7.4\pm1.2)\times10^{-11}$	0.62 ± 0.02

condition is fulfilled, i.e., the correlation of the scattered electric field rather than intensity is detected, due to the presence of stray light, which can act as a local oscillator. It has to be noticed that the scattered light is H polarized while the stray light is mainly V polarized and these two fields cannot interfere. Nevertheless, a small quantity of H-polarized stray light cannot be excluded due to, for instance, a small birefringence in the glass cell, in the sample, and in the optical setup. As a consequence, a small quantity of the heterodyne signal can be present in the spectra, mainly affecting the very long-time behavior. An independent measurement performed at a 90° scattering angle, where the homodyne condition is most likely achieved, verified that the heterodyne contribution is negligible in the central part of the relaxation, and it did not affect the data analysis reported in the following.

For a Gaussian process in the homodyne case the intensity autocorrelation function $G^{(2)}(t)$ is related to the autocorrelation function of the scattered field $g^{(1)}=\langle E(t)E(0)\rangle/\langle|E(0)|^2\rangle$ through the equation [36]

$$G^{(2)}(t)=\langle I\rangle^2(1+f|g^{(1)}(t)|^2), \tag{6}$$

where f is a constant. The spectral width of the intensity autocorrelation function of a glass-forming system is usually larger than that of a single exponential function. So far, the phenomenological function, which better fits the measured data with the lowest number of free parameters is the Kohlrausch-Williams-Watts (KWW) [37] function,

$$g^{(1)}(t)=a\exp[-(t/\tau_{KWW})^{\beta}], \tag{7}$$

where $0<\beta\leqslant1$ is the shape (stretching) parameter. Equations (6) and (7) were used to fit our PCS data and the values of τ_{KWW} and β obtained from this procedure are reported in Table II. In Fig. 5 the set of measured correlation functions is shown together with the KWW fitting functions represented by full lines. The values of the relaxation time and of the stretching parameter obtained by the fitting procedure were used to calculate the average relaxation time

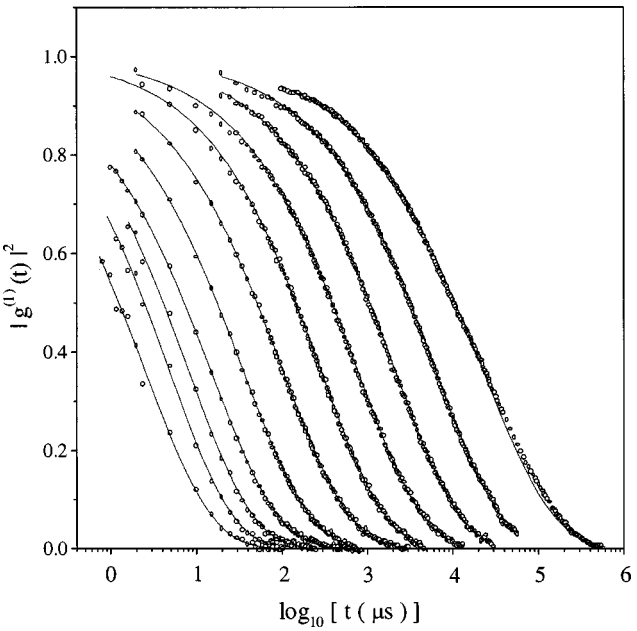

FIG. 5. VH correlation functions measured in back-scattering geometry at 261, 263, 265, 267, 269, 271, 273, 275, 277, 279, and 281 K (from right to left). Solid lines represent the fits to the data using the KWW function of Eq. (7).

$$\langle \tau \rangle = \frac{\tau_{\mathrm{KWW}}}{\beta} \Gamma\left(\frac{1}{\beta}\right), \tag{8}$$

where Γ is the Gamma function. The values of $\langle \tau \rangle$, reported in Table II, are discussed in the following in comparison with the ones obtained from viscosity measurements.

For a direct comparison with dielectric and Fabry-Perot relaxation parameters, the PCS spectra should be also fitted by a HN relaxation function. The fit cannot be as direct as in the case of the KWW function, since the HN is defined in the frequency domain and has no simple analytical form in the time domain. Recently Alvarez, Alegría, and Colmenero [38] have shown that a fitting of KWW functions by HN functions is possible by means of the histogram method introduced by Imanishi, Adachi, and Kodata [39]. Using that iterative procedure, the autocorrelation function $g^{(1)}(t)$ can be calculated by the discrete Laplace transform of a distribution function of retardation times $L(\tau_k)$,

$$g^{(1)}(t) = \sum_{k=0}^{n} L(\tau_k) e^{-t/\tau_k} \Delta, \tag{9}$$

where $\Delta = 10^{\delta/2} - 10^{-\delta/2}$ is the step of the chosen histogram. We used a value $\delta = 0.25$, corresponding to $1/d = 4$ points (relaxation times) per decade. The updated values of the distribution function $L(\tau_k)$ are calculated from those of the imaginary part of the HN susceptibility,

$$\chi''(1/\tau_i) = \mathrm{Im}\{[1 + (i\tau_{\mathrm{HN}}/\tau_i)^{\alpha}]^{-\gamma}\} \tag{10}$$

and from the calculated loss

$$\chi''_{\mathrm{calc}}(1/\tau_i) = \sum_{k=0}^{n} L(\tau_i)[\tau_i/\tau_k + \tau_k/\tau_i]^{-1} \Delta, \tag{11}$$

through the relation

$$L_{\mathrm{new}}(\tau_i) = L_{\mathrm{old}}(\tau_i) + K[\chi''(\tau_i) - \chi''_{\mathrm{calc}}(\tau_i)], \tag{12}$$

where K is a numerical factor whose value was set to 0.3. The calculation of Eqs. (11) and (12) was reiterated until the values of χ''_{calc} and $\chi''(1/\tau_i)$ became sufficiently close to each other. Using this procedure, a best fit of Eq. (9) has been performed to PCS spectra by varying the values of the HN parameters of Eq. (12) and the results are reported in Table II. The HN fitting functions are almost undistinguishable from the KWW ones and both of them seem to be adequate to describe the behavior of $G^{(2)}(t)$ within the experimental error. For this reason the KWW function is usually chosen, since it uses the single shape parameter β rather than the two parameters α and γ of the HN.

As an alternative procedure to compare light scattering and dielectric data, $G^{(2)}(t)$ could be converted to the frequency domain and then fitted by an HN function. However, in this case, the errors of the transformation procedure would add to the experimental ones in a nontrivial way while, by the transformation to the time domain of the HN function, any precision level can be obtained simply by increasing the number of iterations in Eqs. (11) and (12).

D. Viscosity measurements

Frequency dependencies of G' and G'' measured within the frequency range of 0.1–100 rad/s at various temperatures were used to construct master curves representing the broad-range frequency dependencies of these quantities. Only shifts along the frequency scale have been performed. This procedure provided a temperature dependence of shift factors ($\log a_T$ vs T). The low-frequency range of the master dependence of G'' (with $G'' \sim \omega$, indicating the Newtonian flow range) was used to determine the zero shear viscosity at the reference temperature [$\eta_0(T_{\mathrm{ref}}) = G''/\omega$]. Viscosity values related to other temperatures were determined as $\eta_0(T) = \eta_0(T_{\mathrm{ref}}) + \log a_T$. The relaxation time corresponding to the transition between the Newtonian flow range at low frequencies and the glassy range at high frequencies at the reference temperature was determined as $\tau(T_{\mathrm{ref}}) = 2\pi/\omega_c$, where ω_c is the frequency at which the G' and G'' curves cross each other. Relaxation times at other temperatures are given by $\tau(T) = \tau(T_{\mathrm{ref}}) + \log a_T$.

E. Evaluation of errors

The relaxation times and shape parameters obtained by fitting both PCS and FPI spectra are reported in Table II together with the relative errors. The values of these errors have been obtained by means of a Monte Carlo procedure. In particular, starting from each experimental spectrum, a set of one hundred ''synthetic'' data sets have been produced by means of the bootstrap Monte Carlo method [40], where a random fraction of original points are replaced by duplicated original points. Each data set has been fitted by means of the Levenberg-Marquardt method [40], giving a distribution of fitted parameters. The estimate of the error of each parameter has been obtained by the standard deviation of the probability distribution of the fitted parameters.

IV. DISCUSSION

In comparing light-scattering spectra of Figs. 1 and 4(a) with dielectric spectra [Fig. 4(b)], analogies and differences are clearly visible. In both cases the structural relaxation is present, quickly moving toward lower frequencies with decreasing temperature. However, in the case of light-scattering spectra, the α peak is located at lower frequency and there is no signature of the peak related to the secondary relaxation, which can be recognized in the dielectric spectra around 0.1 GHz. This phenomenology is better evidenced in Figs. 6 and 7 by looking at the temperature behavior of the shape parameters and of the characteristic relaxation times, respectively. In fact, although the mutual consistency of dielectric and light-scattering shape parameters confirms that the two techniques are revealing the same α process, the characteristic times are different and the difference increases with temperature. To get a more quantitative evaluation of this trend, both dielectric and light-scattering data were fitted by the VFT law [Eq. (1)]. The values of the parameters obtained by the fit are $\tau_0 = 1.2 \times 10^{-12}$ s, $B = 730$ K, $T_0 = 234$ K for dielectric data [28], and $\tau_0 = 8.17 \times 10^{-12}$ s, $B = 790$ K, $T_0 = 228$ K for light-scattering data. The difference in the high temperature-limiting value of the relaxation time τ_0 accounts for the fact that by increasing the temperature,

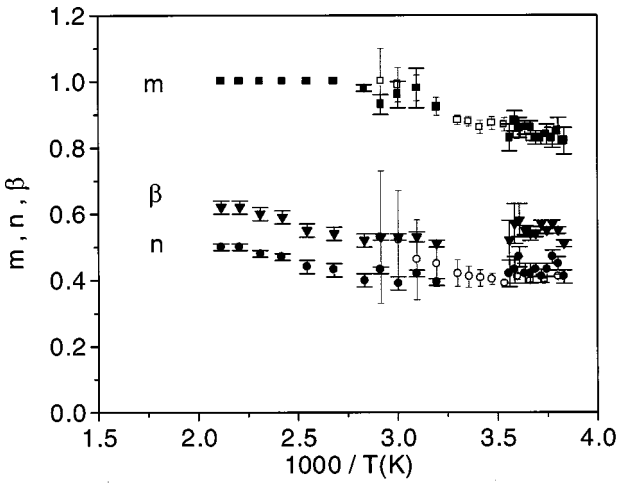

FIG. 6. Temperature behavior of the α-relaxation shape parameters. Solid symbols are depolarized light-scattering data and open symbols are dielectric spectroscopy data from Ref. [28].

the DLS relaxation time becomes progressively longer than the DS one, as visible in Fig. 7.

The observed higher value for the DLS relaxation time cannot be easily interpreted in terms of single-particle rotational diffusion. Theoretically, in the case of the Debye rotational diffusion model, the dielectric relaxation time is three times longer than the light-scattering one [41]. But in the present case as well as, for instance, in polystyrene (PS) [42], DLS relaxation times are much longer than the dielectric ones. In PS the temperature dependence of τ is almost the same for the two techniques and it was deduced that anisotropy fluctuations revealed by light scattering are determined by a much larger molecular subunit than dielectric fluctuations. In the case of DGEBA, an empirical explanation [43] could be attempted in terms of the SED model with a smaller effective hydrodynamic volume [V_h of Eq. (2)] of the part of the molecule that gives rise to the dielectric relaxation (the two epoxy rings at the extremes of the molecule) and a larger radius for the part responsible for light

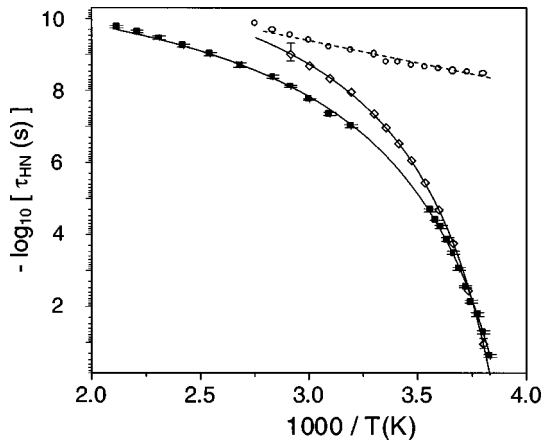

FIG. 7. Temperature behavior of the relaxation time obtained by the HN fit to the depolarized light-scattering spectra (solid symbols) and dielectric spectra from Ref. [28] (open symbols). The structural relaxation data are fitted by a Voghel-Fulcher-Tammann law (solid lines) and the secondary relaxation by an Arrhenius law (dashed line).

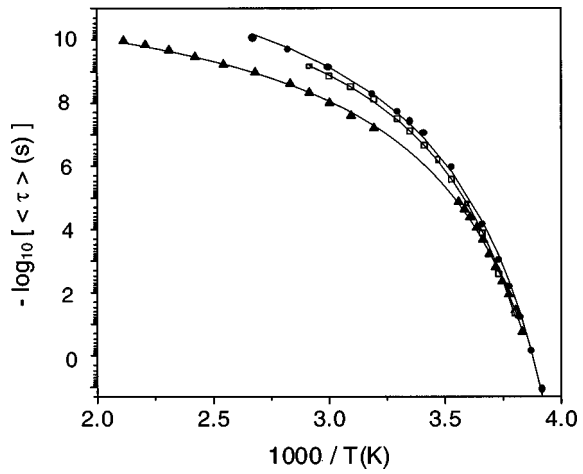

FIG. 8. Average values of the structural relaxation time as a function of temperature. Triangles, squares, and circles refer to depolarized light-scattering, dielectric spectroscopy, and viscosity measurements, respectively, obtained as discussed in the text. The data are fitted by Vogel-Fulcher-Tammann laws (solid lines).

scattering (probably the aromatic rings inside the molecules). In this scheme, the effective volume of the dielectric relaxing unit is constant in the whole temperature range, giving rise to the $\tau \propto \eta$ behavior, while the effective light-scattering volume decreases with decreasing temperature, coming close to the dielectric one when approaching the glass transition. This is a strange and counterintuitive behavior, which deserves a more careful analysis.

A better understanding of the characteristics of the α relaxation of DGEBA revealed by DLS and DS, can be obtained by a quantitative comparison with viscosity data. In the present case of a wide distribution of correlation times, the quantity we compare with viscosity is the average relaxation time. In the case of dielectric and FPI spectra, where an HN relaxation function was used to fit the experimental data, the values of τ_{HN}, α, and γ have been used in Eqs. (10)–(12) to calculate the corresponding distribution of retardation times and, via Eq. (10), the autocorrelation function, which has been fitted by the KWW function of Eq. (7). The average relaxation time has been thus calculated by Eq. (8). The values of τ_{KWW}, β, and $\langle\tau\rangle$ obtained by this procedure are reported in Table II. The dielectric and light-scattering average relaxation times $\langle\tau\rangle$ are reported in Fig. 8, together with the shear relaxation time. Also in this case the relaxation times were fitted by the VFT law of Eq. (1). The values of the obtained parameters are $\tau_0 = 5.17 \times 10^{-12}$ s, $B = 777$ K, and $T_0 = 229$ K for light-scattering data, $\tau_0 = 0.136 \times 10^{-12}$ s, $B = 909$ K, and $T_0 = 227$ K for shear relaxation data, and $\tau_0 = 0.504 \times 10^{-12}$ s, $B = 797$ K, and $T_0 = 232$ K for dielectric data.

To test the applicability of the SED law, the $\log(\langle\tau\rangle)$ vs $\log(\eta)$ is frequently plotted. In the case of DGEBA this plot is reported in Fig. 9, where three interesting features can be recognized: (i) in the whole temperature range the dielectric relaxation data follow the SED law, which in this plot corresponds to the straight line $\tau \propto \eta$, while light-scattering data markedly deviate from this behavior, (ii) in a very wide viscosity and relaxation time range, extending for more than seven decades, the linear behavior of DLS relaxation time in

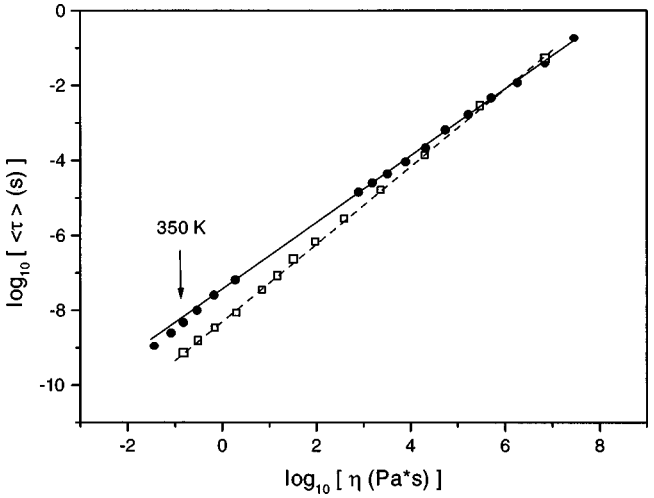

FIG. 9. Log of the average values of the structural relaxation time vs log of viscosity. Solid circles are depolarized light-scattering data and open squares are dielectric spectroscopy data. The dashed line is the $\tau \propto \eta$ behavior while the solid line is $\tau \propto \eta^{0.89}$, which fits the light-scattering data.

the log-log plot of Fig. 9 can be fitted by the power law

$$\tau \propto \eta^{0.89}, \tag{13}$$

and (iii) the light-scattering data depart from the linear behavior at a temperature of about 340–350 K.

Deviations of the α-relaxation time from the SED relation in supercooled liquids are well documented by different experimental techniques [12–20]; our result gives further experimental evidence of such phenomenon.

In previous investigations, many evidences were reported of a decoupling of translational diffusion and reorientational relaxation, and this phenomenon is generally interpreted in terms of the existence in the liquid of both fluidized and correlated regions or domains [19,44,14]. The specific properties of these domains, such as dimension, density, and characteristic lifetime, could not be derived for an *ab-initio* theory and are usually introduced as *ad-hoc* assumptions, which are typically different for different authors (for a recent overview and new hints, see Refs. [16] and [45]). Generally, in these models the translational diffusion decouples from viscosity and rotational diffusion since it involves the passage of molecules through different domains. However, more recent deviations from SED have been reported also for the rotational diffusion, as revealed by dielectric spectroscopy in many glass-forming systems [16].

Our results on DGEBA give some further information on the phenomenology of SED breakdown. In fact, it is generally accepted that both light-scattering and dielectric spectroscopy are sensitive to the rotational dynamics of liquid molecules. In this frame, the contemporary evidence in DGEBA of a SED behavior revealed by DS and of a marked deviation from SED revealed by DLS cannot be easily explained in terms of fluidized or correlated regions. In fact, it would correspond to a situation where different parts of the molecule (epoxy rings revealed by DS and aromatic rings revealed by DLS) belong to different regions of the sample (correlated and fluidized, respectively). This strange behavior suggests the SED model to be inappropriate for describing the light-scattering results when approaching the glass transition.

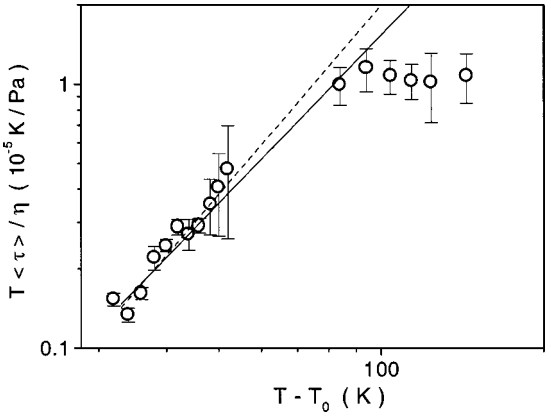

FIG. 10. Temperature behavior of $T\langle\tau\rangle/\eta$ obtained from depolarized light-scattering data. The full line is obtained by fitting $A(T-T_0)^a$ to data at $T \leqslant 323$ K, with T_0 fixed to 229 K, and $a = 2.12 \pm 0.16$. The dashed line is the fit of the PCS data ($T \leqslant 281$ K) giving $a = 2.38 \pm 0.29$.

A model has been recently proposed to explain the SED breakdown in supercooled *o*-terphenyl [26] where starting from a continuum approach, the DLS relaxation time has been related to a correlation volume V_a through the equation

$$\tau \propto \frac{\eta}{V_a T}. \tag{14}$$

To test the suitability of this equation in describing our results, we plot $T\langle\tau\rangle/\eta$ vs T in Fig. 10. It can be seen that for temperatures higher than 313 K, the value of $T\langle\tau\rangle/\eta$ remains almost constant, while a steep decrease occurs for lower temperatures. It is interesting to note that for $T < 313$ K the value m (the low-frequency shape parameter, Fig. 6) becomes lower than 1. This result suggests the presence of an onset of cooperative motions for temperatures lower than 313 K, with a cooperative volume, which increases with decreasing temperature. This interpretation can be pushed forward by assuming the proportionality $V_a \propto \xi_a^3$, where ξ_a is the characteristic length of the dynamic glass transition. [26] The fluctuation theory of the glass transition [5] predicts a divergence of ξ_a for temperatures approaching the Vogel temperature T_0 of Eq. 1, according to the formula

$$\xi_a \propto (T-T_0)^{-\nu}, \tag{15}$$

where $\nu = \frac{2}{3}$ in ordinary space. Therefore, if the correlation length revealed by DLS determines the value of ξ_a, the fluctuation theory predicts that $T\tau/\eta$ must be proportional to $(T-T_0)^2$. The temperature dependence of $T\tau/\eta$ (Fig. 10) was fitted by $(T-T_0)^a$, with T_0 fixed to 229 K, the value deduced by the VFT fit of light scattering, viscosity, and dielectric data. If we use both PCS and C-PTI data the value of a obtained by the fitting procedure amounts to 2.12 ± 0.16. Taking only PCS data, one obtains a higher value of $a = 2.38 \pm 0.29$. One should notice the large errors of the PCS data measured at the highest temperature results from the fact that in the corresponding correlation function the short-

est time part is missing due to usual instrumental limitations. It can be seen that both values of a are consistent within the experimental error. We feel, however, that the lower value of a is more meaningful because it is obtained by a fit to the data in a broader T range and the estimated error in the fit is lower. Moreover, the close correspondence of the values of the Vogel temperature T_0 obtained by different techniques favorably compares with the predictions of the fluctuation theory of glass transition [5]. In fact, the relaxation modes probed by different susceptibilities are expected to be represented by a common set of $\ln(\tau)$ vs T hyperbolas with two common asymptotes, one of which should be T_0.

As a final remark, we notice that our data can be fitted by both the fractional power law (Fig. 9) and by the fluctuation theory (Fig. 10), and that no straightforward analytical relationship exists between Eqs. (13)–(15). The two models cannot be easily derived one from the other and the experimental data cannot discriminate between them. In favor of the latter there is a consistent picture of the temperature behavior of τ close to the glass transition given by the model, opposed to a lack of explicit theoretical derivation of the fractional SED.

In summary, we have reported the results of the depolarized light-scattering experiments performed in liquid and supercooled DGEBA. To access the frequency range between 1 Hz and 300 GHz we combined the spectra obtained from a tandem Fabry-Perot interferometer of different free spectral ranges, a confocal interferometer, and a photon correlation spectroscopy experiment. The temperature evolution of the structural relaxation time obtained by these techniques has been compared with viscosity to test the validity of the SED law, and both the relaxation time and the shape parameters have been compared with dielectric ones, to test how these two different techniques account for the same structural relaxation. Particular attention has been paid to the mutual consistency of the compared quantities, i.e., the same phenomenological relaxation functions were used to fit the different spectra so that a direct comparison of relaxation times and shape parameters could be done. The results obtained confirmed the existence of a change in the dynamics of DGEBA at a temperature of about 90 K higher than the glass-transition temperature previously revealed by both a change in the temperature behavior of the structural relaxation time and a bifurcation of structural and secondary relaxation. [28,24] The presence of such a transition seems to be a peculiar characteristic of fragile glass-forming systems, as recently revealed by different spectroscopic techniques [23,12]. A further interesting feature was evidenced in DGEBA, i.e., a dielectric relaxation time proportional to viscosity, as predicted by the SED law, and a light-scattering relaxation time that violates the SED and follows the fractional behavior $\tau \propto \eta^{0.89}$ for more than seven decades in viscosity and time. As an alternative interpretation of the violation of SED law, following the approach recently proposed for *o*-Terphenyl, the light-scattering relaxation time has been related to the development of correlated volumes in the supercooled system. With the additional hypothesis that the correlation length revealed by DLS determines the value of ξ_a, i.e., the characteristic length of the dynamic glass transition, [26] the value of ξ_a was found to diverge on approaching the Vogel temperature of the system, as predicted by the fluctuation theory of glass transition. Further experiments are presently in progress in our laboratories on epoxy systems of different complexity to test the degree of generality of these findings.

ACKNOWLEDGMENTS

It is a pleasure to thank Professor H. Sillescu for extensive discussions. Partial support of the Deutsche Forschungsgemeinschaft (SFB 262) and INFM, Sezione C, is gratefully acknowledged.

[1] J. Jäckle, Rep. Prog. Phys. **49**, 171 (1986).
[2] H. Vogel, Phys. Z. **22**, 645 (1921); G. S. Fulcher, J. Am. Ceram. Soc. **8**, 339 (1923).
[3] J. D. Ferry, *Viscoelastic Properties of Polymers* (Wiley, New York, 1980).
[4] G. Adam and J. H. Gibbs, J. Chem. Phys. **43**, 139 (1965).
[5] E. J. Donth, *Relaxation and Thermodynamics in Polymers: Glass Transition* (Akademic Verlag, Berlin, 1992).
[6] M. H. Cohen and G. S. Grest Ann. (N.Y.) Acad. Sci. **371**, 199 (1981).
[7] R. Richert and H. Wagner, Proc. SPIE **3181**, 49 (1997); J. Phys. Chem. **99**, 10 948 (1995).
[8] W. Götze and L. Sjögren, Rep. Prog. Phys. **55**, 242 (1992).
[9] See, for instance, H. Z. Cummins, G. Li, W. Du, R. M. Pick, and C. Dreyfus, Phys. Rev. E **55**, 1232 (1997); **53**, 896 (1996); M. J. Lebon, C. Dreyfus, G. Li, A. Aouadi, H. Z. Cummins, and R. M. Pick, *ibid.* **51**, 4537 (1995); H. Z. Cummins, G. Li, W. M. Du, J. Hernandez, and N. J. Tao, J. Phys.: Condens. Matter **6**, (S23) A51 (1994).
[10] W. Steffen, A. Patkowski, H. Gläser, G. Meier, and E. W. Fischer, Phys. Rev. E **49**, 2992 (1994); W. Steffen, A. Patkowski, G. Meier, and E. W. Fischer, J. Chem. Phys. **96**, 4171 (1992).
[11] J. L. Dote and D. Kivelson, J. Phys. Chem. **87**, 3889 (1983).
[12] E. Rössler, Phys. Rev. Lett. **65**, 1595 (1990); Ber. Bunsenges. Phys. Chem. **94**, 392 (1990); J. Chem. Phys. **92**, 3725 (1990).
[13] L. Andreozzi, F. Cianflone, C. Donati, and D. Leporini, J. Phys.: Condens. Matter **8**, 3795 (1996).
[14] G. Tarjus and D. Kivelson, J. Chem. Phys. **103**, 3071 (1995).
[15] J. A. Hodgdon and F. H. Stillinger, Phys. Rev. E **48**, 207 (1993).
[16] I. Chang and H. Sillescu, J. Phys. Chem. B **101**, 8794 (1997).
[17] F. Fujara, B. Geil, H. Sillescu, and G. Fleischer, Z. Phys. B **88**, 195 (1992).
[18] G. Heuberger and H. Sillescu, J. Phys. Chem. **100**, 15 255 (1996).
[19] H. Sillescu, Phys. Rev. E **53**, 2992 (1996).
[20] M. T. Cicerone and M. D. Ediger, J. Chem. Phys. **103**, 5684 (1995).
[21] F. Stickel, E. W. Fischer, and R. Richert, J. Chem. Phys. **102**, 6251 (1995).

[22] F. Stickel, E. W. Fischer, and R. Richert, J. Chem. Phys. **104**, 2043 (1996).
[23] C. Hansen, F. Stickel, T. Berger, R. Richert, and E. W. Fischer, J. Chem. Phys. **107**, 1086 (1997).
[24] S. Corezzi, S. Capaccioli, G. Gallone, A. Livi, and P. A. Rolla, J. Phys.: Condens. Matter **9**, 6199 (1997).
[25] A. P. Sokolov, W. Steffen, and E. Rössler, Phys. Rev. E **52**, 5105 (1995); E. Rössler, A. P. Sokolov, A. Kisliuk, and D. Quitmann, Phys. Rev. B **49**, 14 967 (1994).
[26] E. W. Fischer, E. Donth, and W. Steffen, Phys. Rev. Lett. **68**, 2344 (1992).
[27] C. A. Angell, J. Non-Cryst. Solids **131–133**, 13 (1991).
[28] R. Casalini, D. Fioretto, A. Livi, M. Lucchesi, and P. A. Rolla, Phys. Rev. B **56**, 3016 (1997).
[29] L. Comez, D. Fioretto, L. Verdini, A. Livi, and P. A. Rolla, Proc. SPIE **3181**, 151 (1997).
[30] M. Schulz and E. Donth, J. Non-Cryst. Solids **168**, 186 (1994).
[31] F. Nizzoli and J. R. Sandercock, in *Dynamical Properties of Solids*, edited by G. Horton and A. A. Maradudin (North-Holland, Amsterdam, 1990).
[32] L. Comez, D. Fioretto, L. Verdini, and P. Rolla, J. Phys.: Condens. Matter **9**, 3973 (1997).
[33] J. Gapinski, W. Steffen, A. Patkowski, A. Kilsiuk, and A. P. Sokolov (unpublished).
[34] G. Li, W. M. Du, X. K. Chen, H. Z. Cummins, and N. J. Tao, Physica A **45**, 3867 (1992).
[35] S. Havriliak, Jr. and S. Negami, J. Polym. Sci., Part C: Polym. Symp. **14**, 99 (1966).
[36] B. J. Berne and R. Pecora, *Dynamic Light Scattering* (Wiley, New York, 1976).
[37] G. Williams and D. C. Watts, Trans. Faraday Soc. **66**, 80 (1970).
[38] F. Alvarez, A. Alegría, and J. Colmenero, Phys. Rev. B **47**, 125 (1993); **44**, 7306 (1991).
[39] Y. Imanishi, K. Adachi, and T. Kodata, J. Chem. Phys. **89**, 7593 (1988).
[40] W. H. Press, S. A. Teukolsky, W. T. Vetterling, and B. P. Flannery, *Numerical Recipes* (Cambridge University Press, Cambridge, 1992).
[41] C. J. F. Böttcher and P. Bordewijk, *Theory of Electric Polarization* (Elsevier, Amsterdam, 1973), Vol. II.
[42] G. D. Patterson, in *Dynamic Light Scattering*, edited by R. Pecora (Plenum, New York, 1985), p. 245.
[43] R. Zwamzig and A. K. Harrison, J. Chem. Phys. **83**, 5861 (1985).
[44] F. H. Stilliger and J. A. Hodgnton, Phys. Rev. E **53**, 2995 (1996); **50**, 2064 (1994).
[45] G. Diezemann, J. Chem. Phys. **107**, 10 112 (1997).